Chapter 2

Metallic Glass Honeycombs

Introduction

Due to the fact that they undergo a glass transition and are stable as an undercooled liquid over a large range of temperatures for a significant amount of time, some metallic glasses have the ability to be formed like plastics. In this vein, metallic glasses can be formed independently from the rapid quenching necessary to avoid crystallization unlike die casting or other forms of casting from the liquid state. The thermoplastic properties of metallic glasses have been utilized to create blow-molded parts [37], extrusions of consolidated powders [38], and foams [39] for instance. A series of bulk metallic alloys has been developed for thermal stability and thermoplastic formability having supercooled liquid regions greater then 150°C and casting thicknesses exceeding 15 mm [40]. Recently, it has been shown that one of these metallic glasses ($Zr_{35}Ti_{30}Be_{27.5}Cu_{7.5}$) has a relatively low viscosity in the supercooled liquid region, and therefore, can be plastically formed by injection molding while maintaining the high strength expected from metallic glass [41].

Metallic glasses have also been used to make several types of cellular structures including high strength foams which are capable of inheriting the me-

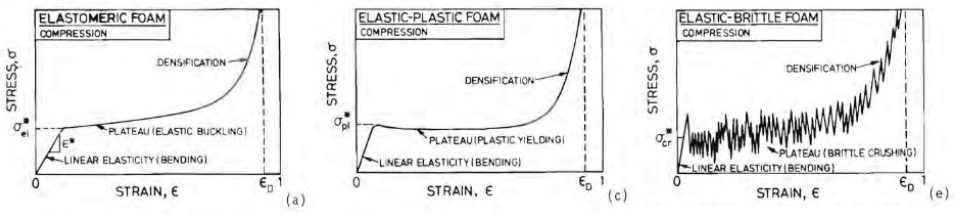

Figure 2.1: Schematic representation of the stress-strain curves of cellular structures in quasi-static compression (from Gibson and Ashby [24]).

chanical properties of the parent metallic glass [36, 42], and metallic glasses with directional porosity [43] or uniaxial porosity[33]. This chapter deals with the fabrication and testing of corrugated sheets and honeycomb structures made by thermoplastic forming of a bulk metallic glass.

Mechanics of Cellular Solids

Schematic stress-strain curves for cellular solids made from different types of materials are shown in figure 2.1 (from reference [24]). Structures with struts yielding by each mechanism exhibit the same general stress-strain behavior with slightly different shapes. Elastic and plastic yielding both show a smooth yielding transition followed by a long, flat stress plateau. Unlike an elastically yielding structure, a plastically yielding structure shows a stress peak before the plateau. The stress-strain curve of a structure whose elements fail by brittle fracture is very rough, showing a sharp peak and a plateau made of many non-catastrophic collapse events. Foams made of metallic glass have been shown to be capable of yielding plastically, but they still exhibit many non-catastrophic collapse events [36]. An example stress-strain curve showing this plastic yielding followed by collapse event behavior is reproduced from Wada and Inoue [29] in figure 2.2.

As discussed in chapter 1, the mechanical properties of cellular solids

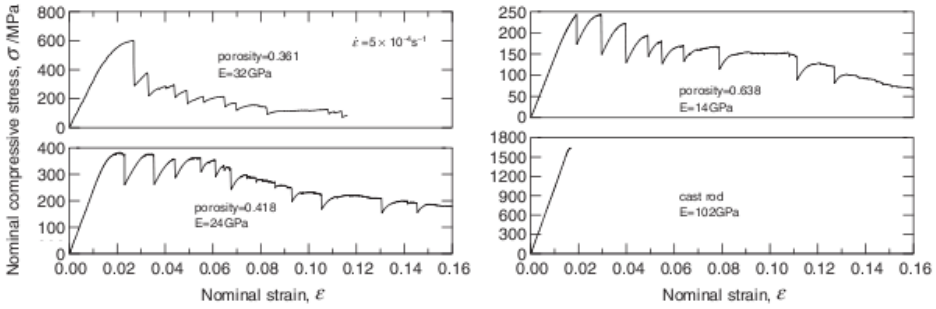

Figure 2.2: Stress-strain response of porous Pd-based bulk metallic glass (from Wada and Inoue [29]).

are determined by several factors including cellular geometry, the properties of the parent material, and the mechanics of the cellular elements in the structure. The strength capabilities of cellular solids follow general semi-empirical relationships of the type:

$$\frac{\sigma^*}{X_s} \simeq C \left(\frac{\rho^*}{\rho_s}\right)^n. \tag{2.1}$$

Following the analysis of Gibson and Ashby [24] for uniaxial in-plane loading of low density honeycombs, equating the load on a strut due to a remote stress with the critical load for buckling gives a yield strength relation for elastic buckling.

$$\frac{\sigma^*}{E_s} \simeq C_1 \left(\frac{\rho^*}{\rho_s}\right)^3. \tag{2.2}$$

Equating the surface stress caused by the resultant moment of a remote stress on the structure with the modulus of rupture of the brittle material gives a relation for elastic-brittle cellular solids.

$$\frac{\sigma^*}{\sigma_{fs}} \simeq C_2 \left(\frac{\rho^*}{\rho_s}\right)^2. \tag{2.3}$$

Equating the maximum moment in the beam due to a remote stress with the

fully plastic moment of the cell wall in bending gives a relation for elastic-plastic cellular solids.

$$\frac{\sigma^*}{\sigma_{ys}} \simeq C_3 \left(\frac{\rho^*}{\rho_s}\right)^2. \tag{2.4}$$

The most important factors in these equations are the material property scaling factors, which largely determine the magnitude of σ^*, and the exponents, which determine how σ^* changes with the relative density. The material scaling properties are especially important as they vary over orders of magnitude with E usually in tens of GPa while σ_{fs} and σ_{ys} range from hundreds of MPa up to several GPa.

The values of the three coefficients (C_1, C_2, and C_3) come from the geometry and mechanics of the analyzed structure. Equations 2.3 and 2.4 differ in the values of their coefficients and the scaling. Examining these coefficients, C_3 is always larger than C_2 because the fully plastic moment in a cellular element,

$$M_p = \frac{1}{4}\sigma_{ys} b t^2, \tag{2.5}$$

where b is the depth of the honeycomb and t is the thickness of a strut, is always smaller than the moment required to cause the surface stress of an element to reach the brittle fracture stress, σ_{fs},

$$M_f = \frac{1}{6}\sigma_{fs} b t^2, \tag{2.6}$$

so if two parent materials, one with σ_{fs} which equals σ_{ys} of the other, the structure that fails by brittle crushing will always have a lower yield stress than the structure that fails by plastic yielding. When experimentally measured relative strengths are plotted against relative density, the results can be compared to the relations presented in equations 2.2 through 2.4 to help in determining the failure mechanism of the cellular solid.

In the case of out-of-plane compressive loading, the elements of the struc-

ture are aligned with the axis of loading, resulting in higher relative strengths as the struts are loaded uniaxially instead of in bending, so the strength-porosity relations are somewhat changed. The out-of-plane properties of honeycombs are not as thoroughly studied, so the strength-porosity relations for these loading conditions are largely empirical. Again, following Gibson and Ashby [24], honeycombs that buckle elastically still have an exponent of $n = 3$ in out-of-plane loading, but the coefficient should be significantly higher ($\sim$20 times higher) than for in-plane loading. Out-of-plane loading for elastic-brittle honeycombs results in a linear relationship between relative strength and relative density which should be a one-to-one relationship if σ_{fs} is measured in compression. On first observation, it would appear that the same would be true for elastic-plastic honeycombs, but the situation is a bit more complex for most honeycombs as the struts tend to undergo plastic buckling. If a honeycomb were to yield plastically without plastic buckling, the relation should be one-to-one. Thorough analysis of this plastic buckling in cell walls by Wierzbicki [44] has shown that minimizing the collapse load with respect to the wavelength of the plastic buckling yields an exponent of $n = 5/3$ in the strength-porosity relationship for out-of-plane plastic collapse of honeycombs.

As described here, the highest relative strengths attainable are those for structures whose elements yield plastically. Metallic glasses in bulk sizes fail by global brittleness, and thin columns are quite susceptible to elastic buckling because of their high elastic limit, but are capable of yielding plastically without catastrophic brittle failure under certain circumstances. As a result of these properties, metallic glass cellular structures can be vulnerable to these less desirable mechanisms of failure, and therefore the design of the structure is critical in optimizing the properties of a metallic glass cellular structure.

To avoid elastic buckling, a structure should contain struts that have slenderness below a critical ratio which can be calculated from the Euler equation for buckling.

$$P_{cr} = \frac{n^2\pi^2 EI}{L^2}, \tag{2.7}$$

$$\sigma_{cr} = \frac{P_{cr}}{A} = \frac{n^2\pi^2 EI}{AL^2} = \frac{n^2\pi^2 E}{(L/r)^2}. \tag{2.8}$$

Set $\sigma_{cr} = \sigma_{ys}$ to get critical slenderness ratio for buckling:

$$\left(\frac{L}{r}\right)_{cr} = n\pi\sqrt{\frac{E}{\sigma_{ys}}}. \tag{2.9}$$

Using E=95 GPa and $\sigma_{ys} = 1750$ MPa for $Zr_{35}Ti_{30}Be_{29}Co_6$

$$\left(\frac{L}{r}\right)_{cr} \simeq 23n, \tag{2.10}$$

n varies between $\frac{1}{2}$ and 2 depending on end conditions, so the critical slenderness ratio varies between roughly 10 and 50.

For metallic glasses, brittle fracture is the dominant failure mechanism, but plastic yielding preempts brittle fracture in bending when the thickness of a cell wall is thinner than the plastic zone size for the alloy. As a result of these design constraints, the structures studied in this chapter were designed to have struts 5 mm long with thickness of 0.5 mm or less. This keeps the struts at the low end of the range of critical slenderness ratios and thin enough that they should yield plastically before fracture.

Another important property of a cellular structure is its ability to absorb energy as it is deformed. Cellular solids absorb energy during deformation by turning mechanical energy into another type of energy (usually thermal energy). This can happen by plastic deformation of the solid or by friction between broken cell walls and struts, as is the case for cellular solids that un-

dergo brittle failure. The energy absorbed per unit volume can be calculated from a stress-strain curve:

$$W = \int_0^{\varepsilon} \sigma(\varepsilon) d\varepsilon, \tag{2.11}$$

which is the area under the stress-strain curve up to ε. Ideally, an energy absorbing structure should have an elastic region, where cell walls bend elastically, followed by an extended plateau with relatively constant stress over a large strain, where energy is absorbed by plastic yielding or brittle fracture, ending in densification as seen in the generalized stress-strain curves in figure 2.1 for three different mechanisms of failure [24]. The majority of the energy absorbed by a cellular structure is absorbed in the plateau region, so maintaining a relatively high and relatively constant plateau stress is important. The rapid increase in stress at densification is due to the fact that the structure has collapsed to the point where the cell walls begin to be pressed against each other. When calculating the useful energy absorbed from a stress-strain curve for a cellular structure, the integral is usually carried out to the densification strain, $\varepsilon_{_D}$, because beyond that point, the experiment is directly testing the behavior of the parent material, and not the cellular structure.

Methods

Ingots of a $Zr_{35}Ti_{30}Be_{29}Co_6$ glass-forming alloy were formed by arc melting in a gettered argon atmosphere using elements of >99.9% purity. This alloy was chosen for its large supercooled liquid region (∼150°C) and its high critical casting thickness (which is slightly higher than the injection molded $Zr_{35}Ti_{30}Be_{27.5}Cu_{7.5}$ alloy mentioned above). From these ingots, amorphous rods with 6 mm diameter were vacuum induction cast using a copper mold.

The amorphous nature of these cast rods was verified using differential scanning calorimetry (DSC) as shown in figure 2.3(a). Using two aligned steel dies and a heated 50-ton hydraulic press, amorphous rods were heated to 430°C (T_g+100) as measured by an attached thermocouple, then pressed until the applied load reached a predetermined limit (usually 48–50 tons). At this temperature and load, the corrugated sheets end up with struts that are 5 mm long and 0.6–0.4 mm thick. The entire die assembly was subsequently water quenched. The entire process was carried out in ambient air and was completed in ∼3 minutes.

Because the forming occurred in ambient air, the surface of the corrugated sheets shows some signs of oxidation, but this appears not to affect the amorphous nature of the corrugated sheets which was also verified using DSC as seen in figure 2.3(b). The forming die, a feedstock amorphous rod and an amorphous corrugated sheet are shown in figure 2.4. The die was designed so that the adjacent struts were at a 60° angle to each other resulting in an equilateral triangle honeycomb-type structure. The amorphous corrugated sheets were cut into strips approximately 5 mm by 35 mm so that the long axis was perpendicular to the ridges in the sheets. Initial mechanical tests resulted in an undesirable brittle failure, so the sheets were heated to 50°C above the calorimetric T_g, held for 2 minutes to equilibrate and quenched in an attempt to capture a higher energy (higher Poisson's ratio) configuration of the glass. DSC of a representative re-equilibrated specimen is shown in figure 2.3(c). In order to achieve a range of low relative densities, some specimens were then thinned using a stirred solution of 45 mL HNO_3:10 mL HF:45 mL H_2O. The HF/HNO_3 solution removed material rather quickly (struts thinned at a rate of approximately 20 μm per minute), but the mass loss appeared macroscopically uniform, and the thinned material remains glassy. A thermal scan of an etched specimen is shown in figure 2.3(d). The thermal analysis shows

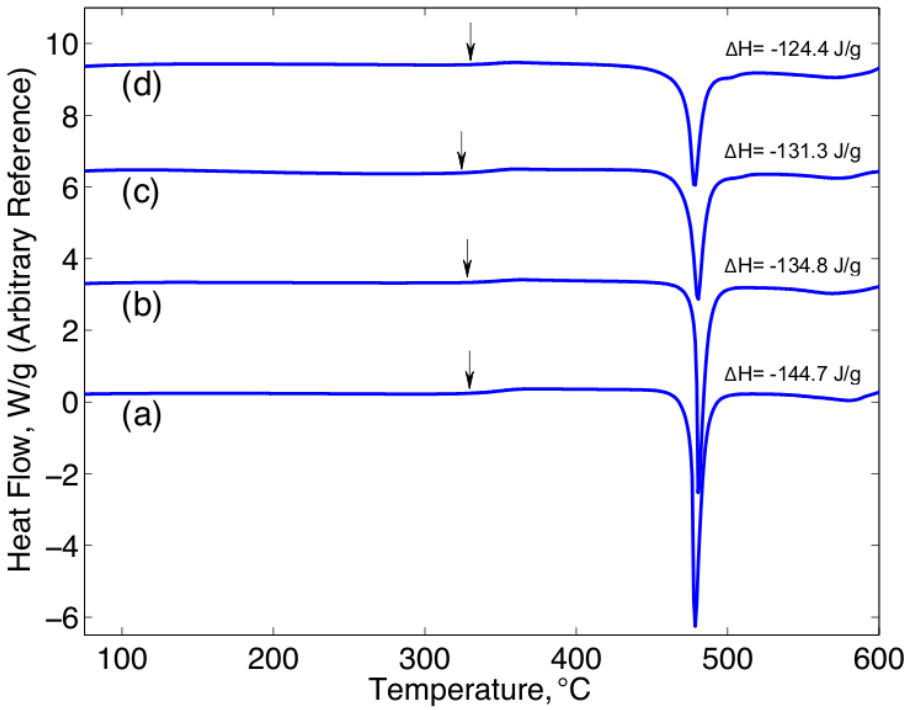

Figure 2.3: Differential calorimetry scans of (a) a feedstock amorphous rod, (b) a corrugated sheet, (c) a sheet etched for 8 minutes, and (d) a corrugated sheet re-equilibrated at 380°C for 2 minutes. The glass transition temperature for each scan is indicated with an arrow, and the enthalpy change shown is that for crystallization.

that while T_g and T_x remain relatively constant, while each subsequent processing step slightly reduces the enthalpy of crystallization. This decrease in ΔH through the processing of a corrugated sheet is about 20 J/g.

The nature of this change in enthalpy of crystallization is not known, but there are several possible explanations. The first, and simplest is that the glass has been partially crystallized. In other Zr-based, Be-bearing metallic glasses, partial crystallization has been observed to cause embrittlement resulting in a severe drop in toughness from $\sim$50 MPa$\sqrt{m}$ to $\sim$5 MPa$\sqrt{m}$ [45]. The structural integrity of these cores and the evidence of plastic deformation discussed below imply that the material is probably not embrittled. Another possibility is that the processing has lowered the configurational enthalpy of the structure. The extra enthalpy in the glass is the product of the ΔC_p between the liquid and the glass and the difference in the temperature from which the glass was quenched. (For the cast rod this is somewhere above the calorimetric T_g, and for the corrugations it is the annealing temperature.) A third possible explanation for this change in enthalpy is the possibility of a phase separation in the glass during the processing steps. A phase separation into two glasses would be an irreversible spinodal type of transformation that would lower the enthalpy of the system resulting in a lower observed enthalpy of crystallization.

These corrugated strips were tested in the in-plane configuration, the z-axis direction in figure 2.5(a), as single cores and as stacks. In both cases, each core was sandwiched between grooved stainless steel plates, each groove corresponding to a node of the corrugation. These plates serve as a means for aligning and confining the nodes of the cores. The stacks were assembled using epoxy, which serves only to hold the stack together prior to mechanical testing. An example of a single core and a multi-core stack are shown in figure 2.5(a) and (b). Single cores were also tested in out-of-plane configuration,

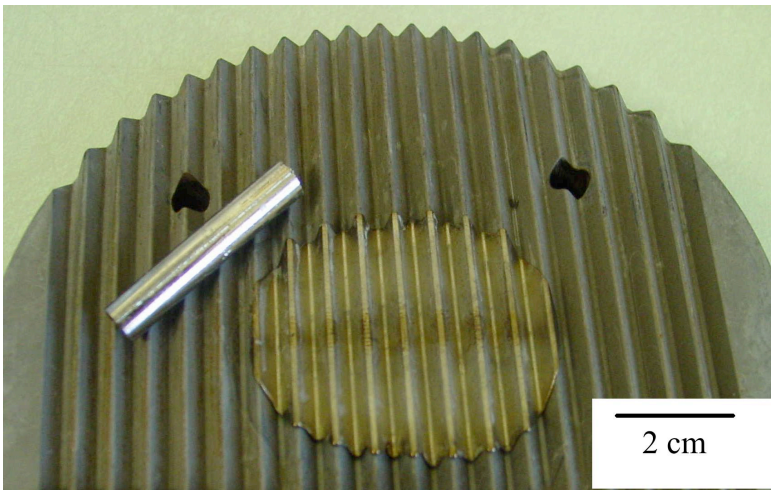

Figure 2.4: Forming die, amorphous feedstock rod, and amorphous corrugated sheet.

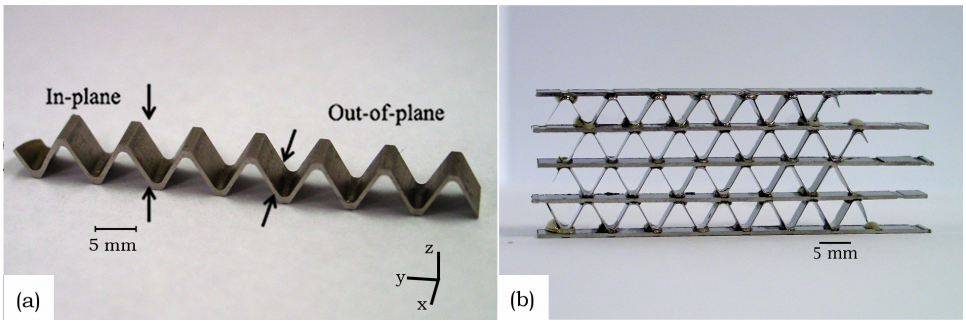

Figure 2.5: (a) Single core as prepared for mechanical testing. The z-axis is the in-plane loading axis, and the x-axis is the out-of-plane loading axis. (b) Assembled stack of four cores with grooved stainless steel horizontal plates with relative density $\rho^* = 0.074$

the x-axis direction in figure 2.5(a), between flat steel plates. Prior to testing, the cut surfaces were ground flat and parallel. All specimens were compressed quasi-statically with an applied strain rate of $10^{-3}s^{-1}$. Tests were carried out with a screw-driven Instron universal testing machine with a load capacity of 50 kN and displacements were measured with a linear variable differential transformer. The relative density of the specimens was calculated using the known geometry of the forming die and the average measured thickness of the struts in a core or stack. The thicknesses of the struts varied by about $\pm 15\%$ from the average measured thickness.

Results

In-Plane Loading

The stress-strain response of quasi-statically loaded single cores is shown in figure 2.6(a). Images of a representative sample during a compression test are shown in figure 2.7(a) through (c). The stress-strain curves typically show an elastic region followed by a short period of plastic deformation leading to a peak in stress. This peak is followed by a substantial stress drop, then a rather low but relatively constant stress plateau. These single cores show significantly higher yield strength than a steel structure of nearly the same relative density (figure 2.6(b)) while maintaing a comparable plateau stress after yielding. Figure 2.7(b) shows that the metallic glass exhibits a significant amount of deformation before the first failure event. Once the first failure event has occurred, the core is still capable of holding load, and portions of the specimen have undergone severe plastic deformation, as can be seen in figure 2.7(c). Micrographs of compressed specimens seen in figure 2.7(d) and (e) also show macroscopic evidence of plastic deformation and shear bands on the tension surface of one strut.

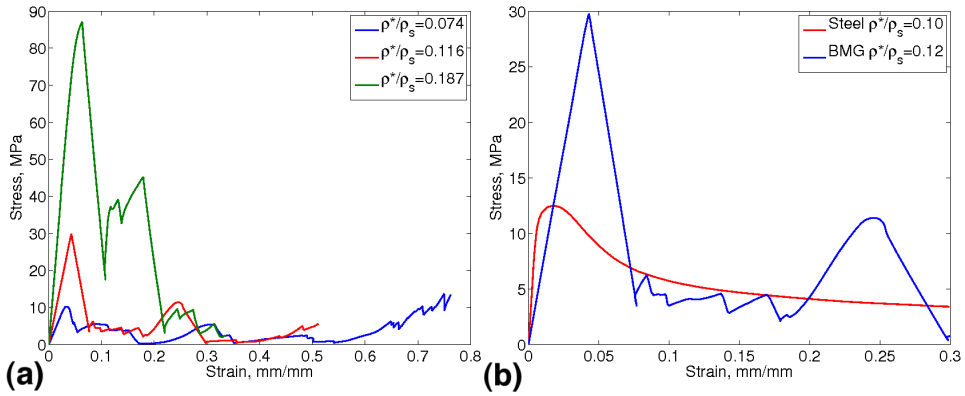

Figure 2.6: (a) Stress-strain response of quasi-statically loaded single cores of corrugated metallic glass of varying relative density. (b) Comparison of stress-strain behavior of BMG core and Steel core of nearly the same relative density. Steel data from Côté et al. [46].

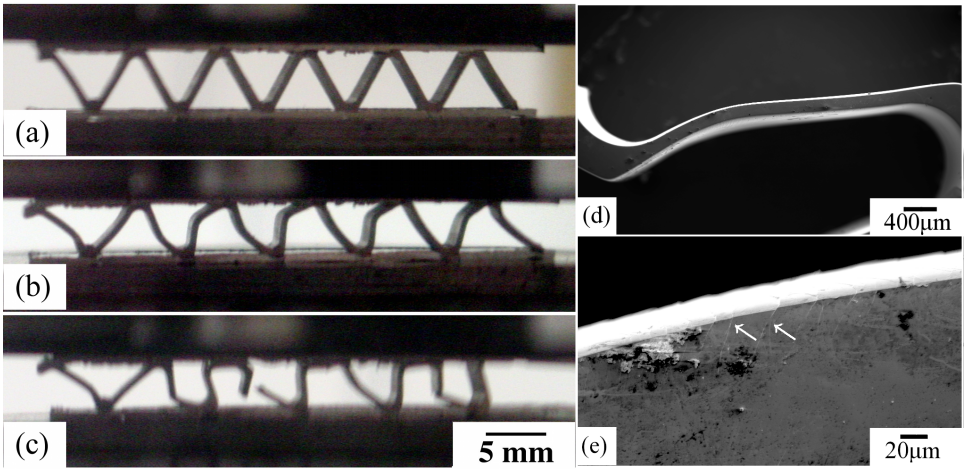

Figure 2.7: Images of a single core during compression testing: (a) elastic region, (b) yielding, (c) after first collapse event, and micrographs of the specimen after compression showing (d) macroscopic plastic deformation and (e) shear bands on the tension surface of the strut, two of which are indicated with white arrows.

The severe stress drop and low plateau stress seen in the single core tests are believed to be a result of the fact that each specimen is composed of around ten struts, therefore, each strut is a critical member, and the fracture of one strut has a quite catastrophic effect on the behavior of the entire core. As seen in figure 2.7(c), the first collapse event in these single cores causes significant rearrangement of the remaining struts which results in a significant reduction in the stability of the structure. One would assume that a structure with more layers or merely more struts would result in a smaller stress drop and a higher plateau stress because fracture of one strut is accommodated by a larger number of remaining struts. The stress-strain response of multi-core stacks, seen in figure 2.8, shows that a structure with more struts actually does show a higher stresses throughout the plateau than do single cores. The curves in figure 2.8(a) and (b) do show a significant stress drop, however, it is followed by a gradually increasing plateau to densification. Upon closer inspection of the stress-strain response in figure 2.6(a) and figure 2.8, there are five or six significant collapse events, each one probably corresponding to the collapse of a single strut, before the onset of densification for the single cores, while the stacked cores with about 30 or 40 struts show around 20 significant collapse events prior to densification. The larger number of collapse events in the stacked structures results in a higher average plateau stress level for a given relative density.

Out-of-Plane Loading

Single cores loaded in the out of plane configuration exhibit the same stress peak followed by an extended lower stress plateau as in-plane specimens, as shown in figure 2.9, but the serrations in the plateau are more regular and the stresses are significantly higher than for in-plane specimens. The out-of-plane configuration loads elements along their axis, so the compressive

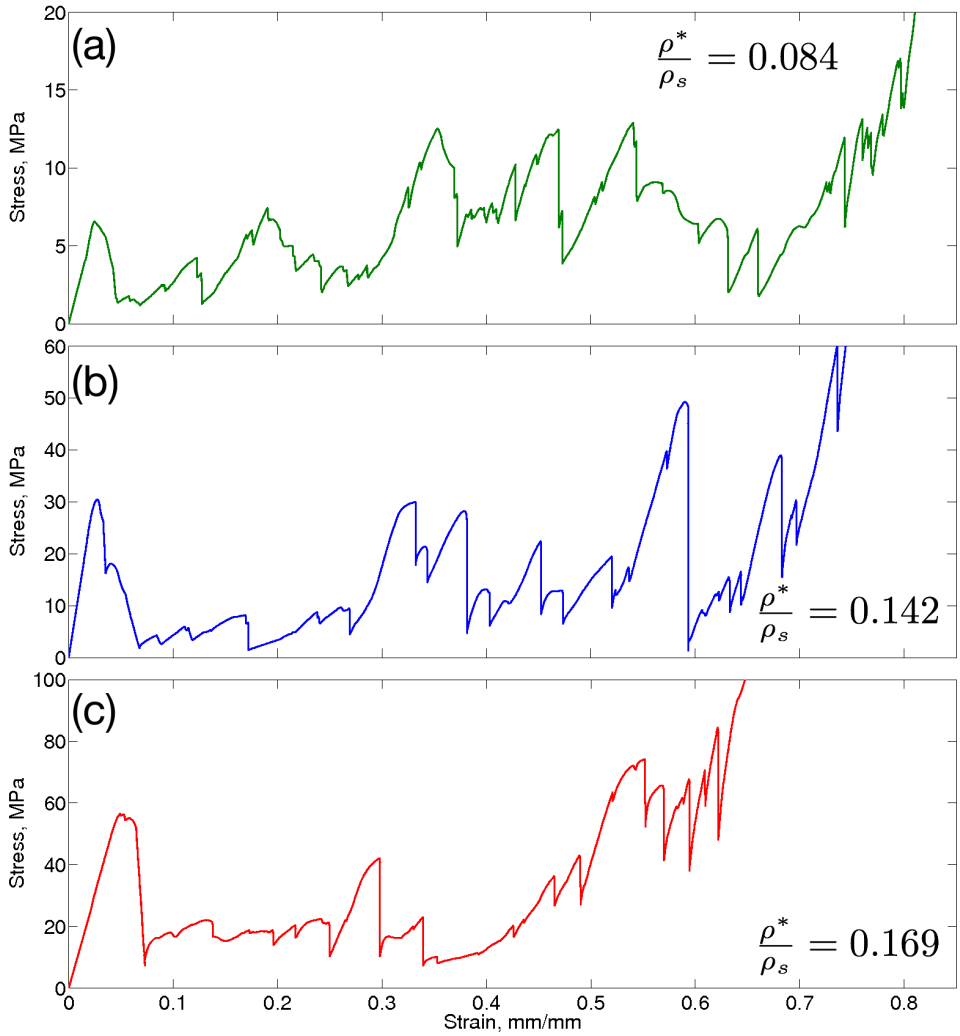

Figure 2.8: Stress-strain response of quasi-statically loaded multi-core stacks of corrugated metallic glass with relative densities of (a) 0.084, (b) 0.142, and (c) 0.169.

strength of the solid material is tested, as opposed to in-plane loading, where the strength of the structure comes from the bending strength of the struts. Figure 2.10(a), (b), and (c) show a single core at several strains during out-of-plane compression. A closer look at the core after the initial collapse event (figure 2.10(b)) shows that the fracture that occurs in these samples spans multiple struts and is oriented at an angle of roughly 45° to the axis of loading. These samples seem to fail as though they were thicker samples and not as though they were a collection of individually yielding struts, as with in-plane loading, one collapse event which affects multiple struts in a sample with a small number of elements causes a significant drop in a stress-strain curve. Despite these collapse events these cores maintain some structural integrity because of the alignment of the elements with the axis of loading, which results in smaller stress drops and a higher stress plateau. The data for a BMG single core are also compared to the stress-strain response of a stainless steel single core of the same relative density in Fig 2.9(b). The metallic glass core shows a significantly higher yield stress and plateau than the stainless steel specimen.

Discussion and Analysis

The relationship between relative strength and relative density for in-plane and out-of-plane metallic glass specimens is shown in figure 2.11(a). The fit lines to the in-plane data for single cores and stacks show exponents of essentially $n = 2$. This along with the microscopic evidence of permanent plastic deformation and multiple shear bands seen in figure 2.7 suggests that these in-plane structures do, indeed, yield plastically, and are, therefore, able to inherit the high yield strength of the parent metallic glass. The strengths of the out-of-plane structures are about 5–10 times higher than for the in-plane

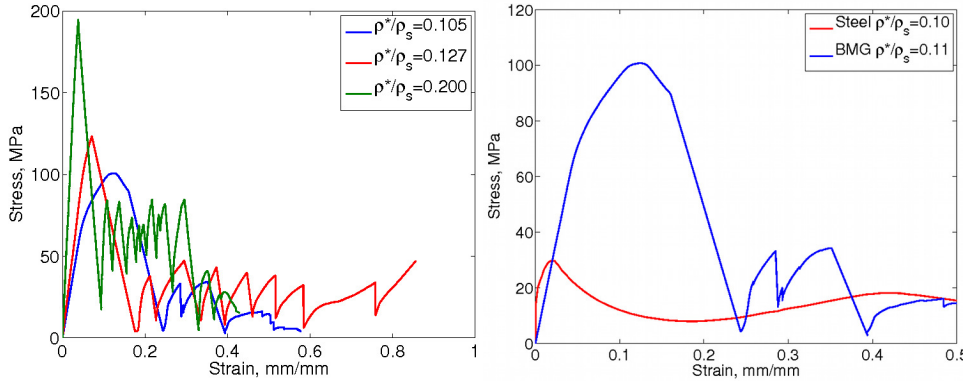

Figure 2.9: (a) Stress-strain response of three out-of-plane quasi-statically loaded metallic glass cores. (b) Comparison of stress-strain behavior of BMG core and Steel core of nearly the same relative density. Steel data from Côté et al. [47].

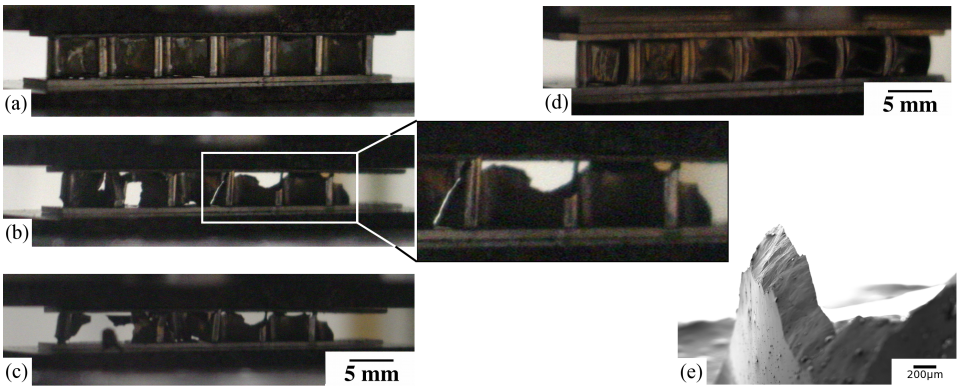

Figure 2.10: Images showing a metallic glass corrugation loaded in compression: (a) in the elastic region, (b) after the first collapse event showing failure that spans several struts at an angle of roughly 45° to the axis of loading, and (c) after several collapse events. (d) A corrugation with $\rho^*/\rho_s = 0.105$ whose struts were thin enough to buckle, and (e) a micrograph of a specimen after out-of-plane compression showing a failure along a single shear band.

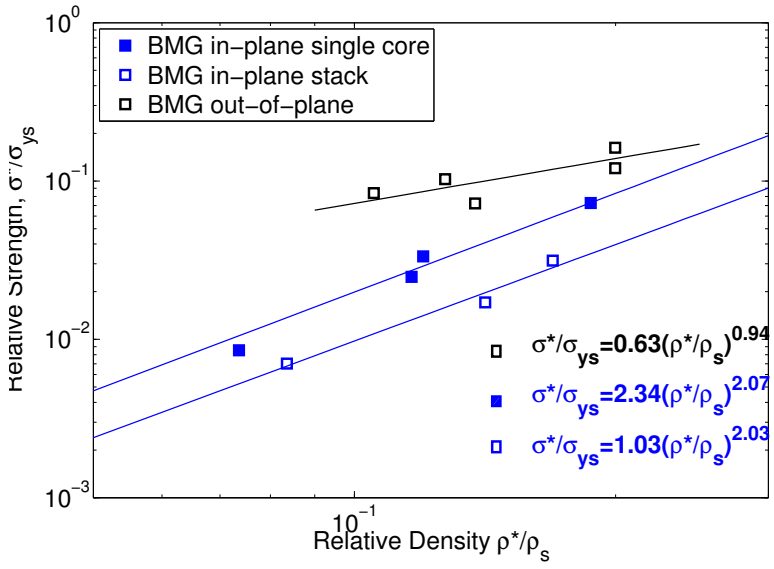

Figure 2.11: Relative strength-relative density plot for metallic glass structures tested in-plane and out-of-plane. Lines are power law best fits to the data.

structures, but the fit line to the out-of-plane data shows an exponent of $n = 0.94$, which is consistent with brittle failure. This assessment is supported by the observation of macroscopic brittle failure in figure 2.10(b) and the lack of shear bands around the fracture surface observed in figure 2.10(e). The corrugated specimen seems to behave more like a specimen that is larger than the plastic zone size of the alloy. As the struts are already well below the plastic zone size for low density structures, the only way to avoid brittle fracture of out-of-plane specimens could be to make the walls thin enough to buckle elastically.

When the strength of the in-plane metallic glass structures is compared to the strength of existing structures of the same geometry made of steel [46], as in figure 2.12(a), we see that the metallic glass specimens have strengths several times higher than the steel structures for the tested relative densities.

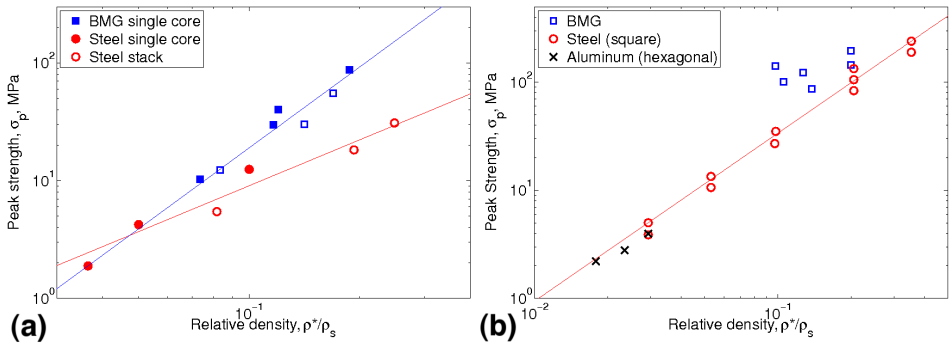

Figure 2.12: Strength-relative density relation for metallic glass and stainless steel cores (closed symbols) and stacks (open symbols) compressed (a) in-plane and (b) out-of-plane. Lines are power law best fits through the data. Steel data from ref. [46, 47].

The yielding mechanism for in-plane metallic glass structures has already been determined to be plastic yielding of the struts, so the greater strength can be attributed to the yield strength of the metallic glass being several times higher than the yield strength of the stainless steel.

The strength-porosity relationships for the out-of-plane metallic glass cores and square stainless steel honeycombs (from Côté et al. [47]) are shown in figure 2.12(b). Much like the in-plane specimens, the out-of-plane metallic glasses exhibit strengths several times higher than the square stainless steel structures. The metallic glass shows a lot of scatter in these strength values, so the fit to the data is not very good, but the data show a loose trend with a relatively low slope. As seen above, these structures have struts that act brittle, but are still very strong.

The energy absorption of the structures was measured by integrating the stress-strain curve from the yield point to the point where the curve increases beyond $\sigma*$ and does not drop below there again. This point corresponds roughly with the densification strain. The area is shown graphically for the

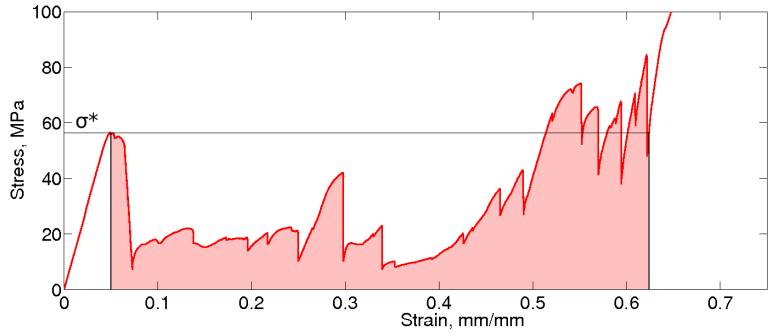

Figure 2.13: Stress-strain curve for a stack of metallic glass cores showing calculation of energy absorbed (shaded area).

stress-strain curve for a stack of metallic glass cores in figure 2.13 and has units of energy per unit volume. In most energy absorbing materials, low weight is desirable, so it is more useful to look at energy absorbed per unit mass. The energy absorption capabilities of the in-plane and out-of-plane structures are compared with those for stainless steel structures [46, 47] in figure 2.14. The metallic glass structures show energy absorption capabilities two orders of magnitude higher than those of the stainless steel structures for in-plane loading, and the data from stacks show higher energy absorption than the single cores. This is due to the larger number of struts in stacks which result in higher sustained stresses in the plateau region of the stress-strain curve. Despite the fact that the out-of-plane specimens appear to fail in a brittle manner, the energy absorption is 10–100 times higher than that for steel square honeycombs of the same density. This high energy absorption is the product of the high yield strength of the metallic glass and the ability of the low-density structure to allow struts to fail without catastrophically collapsing as a whole.

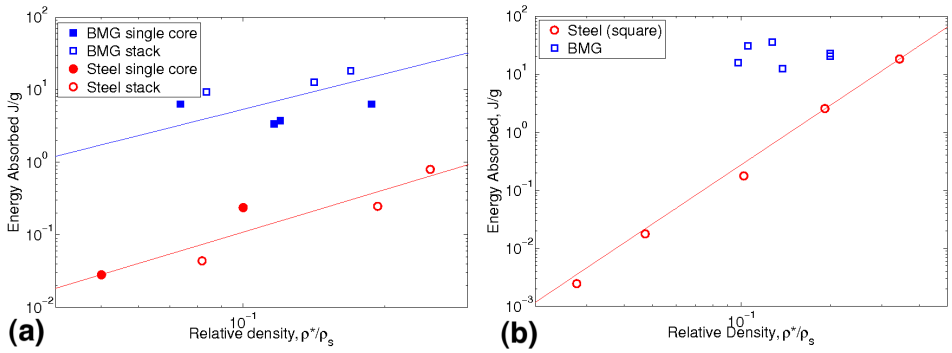

Figure 2.14: Energy absorption diagram for metallic glass cores and stacks and stainless steel structures in (a) in-plane and (b) out-of-plane loading. Lines are power law best fits through the data.

Conclusion

Periodic cellular amorphous metal structures were produced using thermoplastic forming techniques and compressed in both in-plane and out-of-plane configurations. The in-plane specimens were shown to yield by plastic yielding of the individual struts and stacks containing larger numbers of struts were shown to exhibit higher sustained plateau stresses than single cores. Out-of-plane specimens were observed to fail in a brittle manner, but maintained high yield strengths and plateau stresses expected from the metallic glass. These materials also show greater strength and energy absorption capabilities than existing steel structures of similar geometries and relative densities. Specifically, energy absorption measured for metallic glass structures is observed to be higher by 10–100 times than that of steel structures.